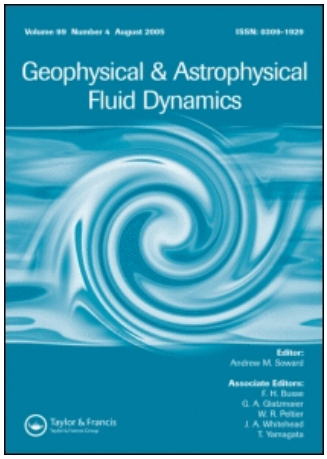

Geophysical & Astrophysical Fluid Dynamics
Publication details, including instructions for authors and subscription information:
http://www.informaworld.com/smpp/title~content=t713642804

Large wavenumber convection in the rotating annulus

A. Abdulrahman [a]; C. A. Jones [a]; M. R. E. Proctor [b]; K. Julien [c]
[a] School of Mathematical Sciences, University of Exeter, Exeter, UK
[b] Department of Applied Mathematics and Theoretical Physics, University of Cambridge, Cambridge, UK
[c] Department of Applied Mathematics, University of Colorado, Boulder, CO, USA

Online Publication Date: 01 December 2000
To cite this Article: Abdulrahman, A., Jones, C. A., Proctor, M. R. E. and Julien, K. (2000) 'Large wavenumber convection in the rotating annulus', Geophysical & Astrophysical Fluid Dynamics, 93:3, 227 - 252
To link to this article: DOI: 10.1080/03091920008204125
URL: http://dx.doi.org/10.1080/03091920008204125

Geophys. Astrophys. Fluid Dynamics, Vol. 93, pp. 227–252
Reprints available directly from the publisher
Photocopying permitted by license only

LARGE WAVENUMBER CONVECTION IN THE ROTATING ANNULUS

A. ABDULRAHMAN[a], C. A. JONES[a,*], M. R. E. PROCTOR[b] and K. JULIEN[c]

[a]*School of Mathematical Sciences, University of Exeter, Exeter EX4 4QE, UK;* [b]*Department of Applied Mathematics and Theoretical Physics, University of Cambridge, Cambridge CB3 9EW, UK;* [c]*Department of Applied Mathematics, University of Colorado, Boulder CO 80309, USA*

(Received 5 April 2000; In final form 31 August 2000)

The annulus model considers convection between concentric cylinders with sloping endwalls. It is used as a simplified model of convection in a rapidly rotating sphere. Large azimuthal wavenumbers are preferred in this problem, and this has been exploited to develop an asymptotic approach to nonlinear convection in the annulus. The problem is further reduced because the Taylor-Proudman constraint simplifies the dependence in the direction of the rotation vector, so that a nonlinear system dependent only on the radial variable and time results. As Rayleigh number is increased a sequence of bifurcations is found, from steady solutions to periodic solutions and 2-tori, typically ending in chaotic behaviour. Both the magnetic (MHD convection) and non-magnetic problem has been considered, and in the non-magnetic case our bifurcation sequence can be compared with those found by previous two-dimensional numerical simulations.

Keywords: Convection; Magnetoconvection; Rotating fluids; Annulus model

1. INTRODUCTION

Convection in the presence of rapid rotation is one of the important problems in geophysical and astrophysical fluid dynamics. It has applications both to the dynamics of the planetary cores, where it is believed to generate magnetic fields (*e.g.* Jones, 2000), and to

*Corresponding author. e-mail: c.a.jones@exeter.ac.uk

planetary atmospheres, where it is believed to generate the complex zonal jet flows (*e.g.* Busse, 1983). Direct numerical simulations of the fully three-dimensional problem have not yet been able to reach the very low values of the Ekman number appropriate to the astrophysical applications, and so our understanding of the problem is still very incomplete. The linear theory of convection in spherical geometry has been studied by Roberts (1968), Busse (1970) and Soward (1977). Recently, Jones *et al.* (2000) have solved the internally heated problem in the limit of small Ekman number, but there are still some unanswered problems when convection sets in first near a boundary. Nonlinear computational studies have been made by Zhang (1991), Sun *et al.* (1993), and some relevant experiments made by Olson and Glatzmaier (1995). Near onset, convection at moderate Prandtl number is manifested in the form of drifting columnar rolls called 'thermal Rossby waves'. In order to study the nonlinear properties of convection the annulus model has been used by Busse and co-workers, and has been reviewed by Busse (1994); the most directly relevant of these papers to the present work is that of Lin, Busse and Ghil (1989) subsequently referred to as LBG89. The annulus model has also been studied at moderately large Rayleigh number and moderately small Ekman number by Brummel and Hart (1993), subsequently referred to as BH93. Since the annulus with inclined top and bottom boundaries is convenient, while still representing the fundamental dynamical features of the planetary systems, it is preferred in this study. Moreover, the annulus model allows comparison with laboratory experimental results that were performed either on the Earth using centrifugal buoyancy (Carrigan and Busse, 1983), or in space using electrostatic radial buoyancy (Hart *et al.*, 1986). In the annulus model, the small gap approximation is often employed allowing curvature to be neglected so that Cartesian coordinates with the azimuthal direction, x, extending to infinity are used. The rapid rotation of the annulus makes the motion of the fluid almost independent of the z direction by the Taylor-Proudman theorem, simplifying the model further. Using the Galerkin method to study numerical solutions for the convection, Busse and Or (1986) found time dependent convection columns, the thermal Rossby waves, and the generation of zonal mean flows similar to those observed in laboratory experiments. Coriolis force plays an important role in producing zonal shearing in the

annulus. The sloping of the axisymmetric end lids with respect to the equatorial plane breaks the geostrophic balance and affects the dynamics of the fluid substantially.

The first bifurcation is normally to steady, drifting, columnar rolls. As the Rayleigh number is further increased a secondary symmetry-breaking bifurcation was found by Or and Busse (1987), also discussed by Busse (1986) and LBG89. This secondary bifurcation is known as the 'mean-flow' instability, as its characteristic effect is to break the symmetry of the mean flow induced by the drifting columns. LBG89 also found chaotic behaviour at larger values of the Rayleigh number. BH93 investigated the same system with a numerical study. The radial and azimuthal directions were accurately resolved, the z-dependence being averaged, as normal in the annulus model. The resulting equations were integrated forward in time. They found the mean-flow instability, and again found chaotic behaviour at higher Rayleigh number, though the bifurcation sequence to chaos was via a quasi-periodic 2-torus, different from the period doubling sequence found by LBG89.

In this paper, we show that a considerable simplification arises if we consider large azimuthal wavenumber motions, which is an appropriate limit in rapidly rotation convection and magnetoconvection, provided the field strength is not too large. This approach, which is related to that given by Bassom and Zhang (1994) for the rotating Bénard problem, allows us to explore the nonlinear regime while still solving differential equations in only the radial variable and time. This allows us to make a detailed investigation of the bifurcation structure of the mean flow at large wavenumber and to understand the transition to turbulent behaviour. We consider first the nonmagnetic case, and then the effect of a uniform magnetic field in the x-direction, which corresponds to an azimuthal field in the annulus. This case was first considered by Busse (1976); see also Petry *et al.* (1997).

2. DERIVATION OF THE EQUATIONS

We consider fluid moving inside an annulus with inclined top and bottom lids. The width of the annulus is D and the height at the centre is L. A vertical cross section of the annulus is shown in Figure 1 to illustrate the problem. The annulus is rotating with angular velocity Ω.

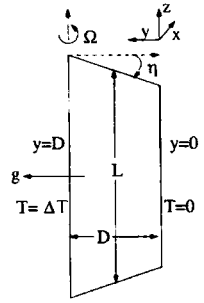

FIGURE 1 A cross section of the annulus.

The endwalls of the annulus are inclined to the horizontal at a small angle η. A temperature difference ΔT is maintained between the inside and outside walls, y is in the radial direction increasing as you go to the rotation axis, with $y=0$ on the outer side of the annulus, and $y=D$ on the inside of the annulus, x increases in the easterly direction. The gravity force g is acting on the direction of increasing y, and the direction of rotation is the direction of increasing z. The condition of no-normal-flow leaving the annulus through the inclined ends is

$$u_y \sin\eta \mp u_z \cos\eta = 0 \quad \text{or} \quad u_y\eta = \pm u_z \quad \text{on} \quad z = \pm \tfrac{1}{2}L,$$

since the inclination η is small. We also assume that the magnetic field is sufficiently weak that the velocity $\mathbf{u}$ is predominantly geostrophic, so we can write

$$\mathbf{u} = -\nabla \times \psi(x,y,t)\hat{\mathbf{z}} + \mathbf{v}',$$

where $\mathbf{v}'$ is the small ageostrophic part of the flow (LBG89). Then $\hat{\mathbf{z}}\cdot\nabla\times$ of the momentum equation gives

$$\frac{\partial\omega}{\partial t} + \frac{\partial(\psi,\omega)}{\partial(x,y)} - 2\Omega\frac{\partial w}{\partial z} = -\hat{\mathbf{z}}\cdot\nabla\times g\alpha\theta\hat{\mathbf{y}} + \frac{1}{\rho}\hat{\mathbf{z}}\cdot\nabla\times(\mathbf{J}\times\mathbf{B}) + \nu\nabla^2\omega,$$

where w is the small ageostrophic vertical velocity, which is $O(\eta)$ (Busse and Or, 1986).

At leading order in η,

$$u_x = -\frac{\partial\psi}{\partial y}, \quad u_y = \frac{\partial\psi}{\partial x},$$

as in the geophysical literature[1] and consistent with Brummel and Hart (1993). Here ω is the vertical vorticity. Integrating over z and applying the boundary conditions allows us to remove w from the problem giving

$$\frac{\partial \omega}{\partial t}+\frac{\partial(\psi,\omega)}{\partial(x,y)}-\frac{4\eta\Omega}{L}\frac{\partial \psi}{\partial x}=-g\alpha\frac{\partial \theta}{\partial x}+\frac{1}{\rho}\hat{\mathbf{z}}\cdot\nabla\times(\mathbf{J}\times\mathbf{B})+\nu\nabla^2\omega.$$

Temperature is taken as $T=\theta+\Delta T y/D$, and magnetic field is taken as $\mathbf{B}=\nabla\times(A+B_0 y)\hat{\mathbf{z}}$, where both θ and A are independent of z. The temperature equation is

$$\frac{\partial \theta}{\partial t}+\frac{\partial(\psi,\theta)}{\partial(x,y)}=-\frac{\Delta T}{D}\frac{\partial \psi}{\partial x}+\kappa\nabla^2\theta.$$

The induction equation gives

$$\frac{\partial A}{\partial t}+\frac{\partial(\psi,A)}{\partial(x,y)}=-B_0\frac{\partial \psi}{\partial x}+\lambda\nabla^2 A.$$

Non-dimensionalising on a length scale D, a time-scale D^2/ν, a temperature $\nu\Delta T/\kappa$ and a magnetic field $\nu B_0/\lambda$, we get

$$\frac{\partial \omega}{\partial t}+\frac{\partial(\psi,\omega)}{\partial(x,y)}-\beta\frac{\partial \psi}{\partial x}=-R\frac{\partial \theta}{\partial x}+Q\left[\frac{\partial J}{\partial x}+P_m\frac{\partial(J,A)}{\partial(x,y)}\right]+\nabla^2\omega, \quad (1)$$

$$P_r\left[\frac{\partial \theta}{\partial t}+\frac{\partial(\psi,\theta)}{\partial(x,y)}\right]=-\frac{\partial \psi}{\partial x}+\nabla^2\theta, \quad (2)$$

$$P_m\left[\frac{\partial A}{\partial t}+\frac{\partial(\psi,A)}{\partial(x,y)}\right]=-\frac{\partial \psi}{\partial x}+\nabla^2 A \quad (3)$$

with

$$\nabla^2 A=-J, \qquad \nabla^2\psi=\omega,$$

$$u_x=-\frac{\partial \psi}{\partial y}, \quad u_y=\frac{\partial \psi}{\partial x}, \quad B_x=\frac{\partial A}{\partial y}, \quad \text{and} \quad B_y=-\frac{\partial A}{\partial x}.$$

[1]Historical note: Lamb, Gill and Pedlosky use $\mathbf{u}=-\nabla\times\psi\hat{\mathbf{z}}$; Batchelor, and Landau & Lifshitz use $\mathbf{u}=\nabla\times\psi\hat{\mathbf{z}}$, so you cannot win. In geophysical problems ψ is often associated with pressure and if you take $\psi\sim p$ you get $\mathbf{u}=-\nabla\times\psi\hat{\mathbf{z}}$.

The dimensionless parameters are defined as follows:

$$P_r = \frac{\nu}{\kappa}, \quad P_m = \frac{\nu}{\lambda}, \quad R = \frac{g\alpha\Delta T D^3}{\kappa\nu}, \quad Q = \frac{B_0^2 D^2}{\mu\rho_0\nu\lambda}, \quad \beta = \frac{4\eta\Omega D^3}{L\nu},$$

where P_r is the Prandtl number, P_m is the magnetic Prandtl number, R is the Rayleigh number, and Q is the Chandrasekhar number. The parameter β is related to the inverse of the Ekman number $E = \nu/2\Omega D^2$ in spherical geometry, where then D is a typical length scale, often the radius of the sphere. In rapidly rotating magnetoconvection, an important parameter is the Elsasser number Λ. In our annulus geometry, Λ corresponds to the combination Q/β.

2.1. Large β Scalings

Let $\beta = \varepsilon^{-3}$, where $\varepsilon \ll 1$. We scale the coordinate $x = \varepsilon\xi$, and time in the frame moving with the wave at speed c_0 so that

$$\frac{\partial}{\partial t} \longrightarrow -\varepsilon^{-2} c_0 \frac{\partial}{\partial \xi} + \frac{\partial}{\partial t}.$$

We now expand the dependent variables ψ, θ and A as

$$\psi = \varepsilon\psi' + \varepsilon\bar{\psi}(y,t), \quad \theta = \varepsilon^2\theta' + \varepsilon^2\bar{\theta}(y,t), \quad A = \varepsilon^2 A' + \varepsilon^2\bar{A}(y,t),$$

where the barred quantities correspond to the average over the x-direction, and the dashed quantities the parts fluctuating in x in zero mean. We write

$$\psi' = \psi_0 + \varepsilon^2\psi_2 + \cdots, \qquad \theta' = \theta_0 + \varepsilon^2\theta_2 + \cdots,$$
$$A' = A_0 + \varepsilon^2 A_2 + \cdots,$$

and

$$\psi_0 = \hat{\psi}\exp ik\xi + \text{c.c.}, \qquad \theta_0 = \hat{\theta}\exp ik\xi + \text{c.c.},$$
$$A_0 = \hat{A}\exp ik\xi + \text{c.c.},$$

where c.c. denotes the complex conjugate of the preceding term. Moreover, we write the parameters in the form

$$Q = \varepsilon^{-2} q, \quad R = \varepsilon^{-4} r, \quad \text{where } r = r_0 + \varepsilon^2 r_2 + \cdots.$$

The leading order in ε is $O(\varepsilon^{-3})$ for the momentum equation (1), and O(1) for the temperature and induction Eqs. (2) and (3), which give

$$\hat{\theta} = \frac{-ik\hat{\psi}}{k^2 - ikc_0P_r}, \quad \hat{A} = \frac{-ik\hat{\psi}}{k^2 - ikc_0P_m},$$

and the dispersion relation governing small disturbances,

$$r_0 = \frac{k^2q(k^2 - ikc_0P_r)}{(k^2 - ikc_0P_m)} + (k^2 - ikc_0P_r)(k^2 - ikc_0 + i/k). \tag{4}$$

The leading order critical Rayleigh number is r_0, but as we see below, bifurcation to a non-trivial solution occurs at a value of r which is $O(\varepsilon^2)$ greater than r_0. The next nontrivial order is $O(\varepsilon^{-1})$ for the momentum equation, and $O(\varepsilon^2)$ for the temperature and induction equations. At this order we derive equations for the mean quantities $\bar{\psi}$, $\bar{\theta}$ and $\bar{A}$ and for the fluctuating quantities ψ_2, θ_2 and A_2. The equations for the fluctuating parts are inhomogeneous, so there is a solvability condition which gives the amplitude equation

$$a_1(\hat{\psi}_t + ik\bar{u}\hat{\psi}) = a_2\hat{\psi}_{yy} + a_3(r_2 + r_0P_r\bar{\theta}_y)\hat{\psi} + a_4\bar{A}_y\hat{\psi}, \tag{5}$$

where

$$a_1 = k^2 + \frac{r_0P_r}{(k - ic_0P_r)^2} - \frac{qP_mk^2}{(k - ic_0P_m)^2},$$

$$a_2 = 2k^2 - ikc_0 + \frac{r_0}{(k - ic_0P_r)^2} - \frac{ic_0kqP_m}{(k - ic_0P_m)^2},$$

$$a_3 = \frac{k}{k - ic_0P_r}, \quad a_4 = \frac{-2P_mk^3q}{k - ic_0P_m}, \quad \text{and} \quad \bar{u} = -\frac{\partial\bar{\psi}}{\partial y}.$$

Here $\bar{u}(y, t)$ is the mean flow in the azimuthal x-direction. The mean equations give

$$\bar{\psi}_t = \bar{\psi}_{yy} + \left(1 - \frac{qP_m}{k^2 + c_0^2P_m^2}\right)ik(\hat{\psi}\hat{\psi}_y^* - \hat{\psi}^*\hat{\psi}_y), \tag{6}$$

$$P_r\bar{\theta}_t = \bar{\theta}_{yy} + \frac{2k^2P_r}{k^2 + c_0^2P_r^2}(\hat{\psi}\hat{\psi}_y^* + \hat{\psi}^*\hat{\psi}_y), \tag{7}$$

$$P_m \bar{A}_t = \bar{A}_{yy} + \frac{2k^2 P_m}{k^2 + c_0^2 P_m^2} (\hat{\psi}\hat{\psi}_y^* + \hat{\psi}^* \hat{\psi}_y), \tag{8}$$

where $*$ denotes the complex conjugate. The $O(\varepsilon^{-1})$ mean momentum equation actually gives an equation for $\bar{\psi}_{yy}$; (6) is the second integral with respect to y. The first integral gives an equation for the mean flow $\bar{u}$

$$\bar{u}_t = \bar{u}_{yy} + \left(1 - \frac{qP_m}{k^2 + c_0^2 P_m^2}\right) ik(\hat{\psi}\hat{\psi}_{yy}^* - \hat{\psi}^* \hat{\psi}_{yy}) \tag{9}$$

which can be used as an alternative to (6).

2.2. Method of Solution

The system of the four nonlinear coupled time-dependent Eqs. (5), (6), (7) and (8) is one-dimensional in space. We solve the system subject to the stress-free boundary conditions (with constant temperature and no normal flow)

$$\hat{\psi} = \frac{\partial \bar{u}}{\partial y} = \hat{\theta} = \bar{A} = 0 \qquad \text{at} \quad y = 0, 1.$$

We have obtained numerical nonlinear solutions for our system subject to the appropriate boundary conditions by implementing a NAG library routine based on finite differences to discretise the space variable, and the method of lines to reduce the system of partial differential equations to a system of ordinary differential equations. The resulting system is solved using a backward differentiation formula method. Our calculations were checked using an independently constructed code based on IDL.

Since we solve the $\bar{\psi}$-equation (6), we must replace the boundary condition $\bar{u}_y = 0$ on $y = 0$, 1 with a boundary condition on $\bar{\psi}$. From (6), $\bar{\psi}_t = 0$ at the boundaries, since $\bar{u}_y = 0$ implies $\bar{\psi}_{yy} = 0$ there. This implies that $\bar{\psi}$ must be constant on the boundaries, and we can set these constants to be zero without loss of generality. This corresponds to setting the y-average of the mean flow $\bar{u}$ to be zero, which can always be achieved by making a Galilean transformation of the coordinate system $x \to x - u_0 t$, where u_0 is any non-zero y-average of the mean flow. Using $\bar{\psi}$ rather than $\bar{u}$ removes the appearance of

second derivatives of $\hat{\psi}$ which occurred in (9), and so the equation system is reduced to the standard form for coupled parabolic equations.

3. NON-MAGNETIC SOLUTIONS

We consider first the non-magnetic case. The reason for that is twofold: first, we want to compare our results with previously published work on this case, namely LBG89 and BH93. Second, we can only elucidate the effects of the magnetic field when the non-magnetic case is reasonably well understood.

From the dispersion relation (4) we can separate the real and imaginary parts; the real part is

$$r_0 = \frac{k^2 q(k^4 + k^2 c_0^2 P_r P_m)}{k^4 + k^2 c_0^2 P_m^2} + k^4 - k^2 c_0^2 P_r + c_0 P_r,$$

and the imaginary part is

$$\frac{k^5 q c_0 (P_m - P_r)}{k^4 + k^2 c_0^2 P_m^2} + k - k^3 c_0 (1 + P_r) = 0,$$

the two equations giving r_0 and c_0 as functions of k.

We deduce the non-magnetic dispersion relation from the magnetic one by setting q to zero in these relations. Then, we compute the critical Rayleigh number by setting

$$\frac{\partial r_0}{\partial k} = 0,$$

giving

$$k = \left(\frac{P_r^2}{2(1+P_r)^2}\right)^{1/6}, \qquad r_0 = 3\left(\frac{P_r^2}{2(1+P_r)^2}\right)^{2/3},$$
$$c_0 = \left(\frac{2}{P_r^2(1+P_r)}\right)^{1/3}.$$

These values, derived by Busse (1970), are used to determine the coefficients a_1 to a_4 in (5).

3.1. Initial Bifurcations

We first consider the bifurcation sequence that occurs as the parameter of supercriticality, r_2, is increased. For simplicity, we first consider the value $P_r = 1$; this value was also used in previously published papers. For $r_2 < \pi^2/2$ the only solution of (5), (6) and (7), with $A = 0$, is the trivial solution. For r_2 slightly bigger than $\pi^2/2$, we find a nontrivial symmetric solution in which the mean quantities $\bar{u}$ and $\bar{\theta}$ are steady and $\hat{\psi}$ undergoes sinusoidal oscillation corresponding to traveling waves of constant amplitude. This solution, like the others in this section, was found by integrating (5), (6) and (7) forward in time until initial transients had disappeared. This solution is a stable solution that continues to exhibit symmetry and steadiness with increasing r_2 up until $r_2 = 15.22$. This symmetry is described by

$$\hat{\psi}(y) = \hat{\psi}(1-y), \quad \bar{u}(y) = \bar{u}(1-y), \quad \text{and} \quad \bar{\theta}(y) = -\bar{\theta}(1-y). \quad (10)$$

As r_2 increases, a second bifurcation occurs at $r_2 = 15.22$ where the system undergoes a symmetry-breaking pitchfork bifurcation. The symmetric solution at $r_2 = 15$ is shown as a solid curve in Figure 2,

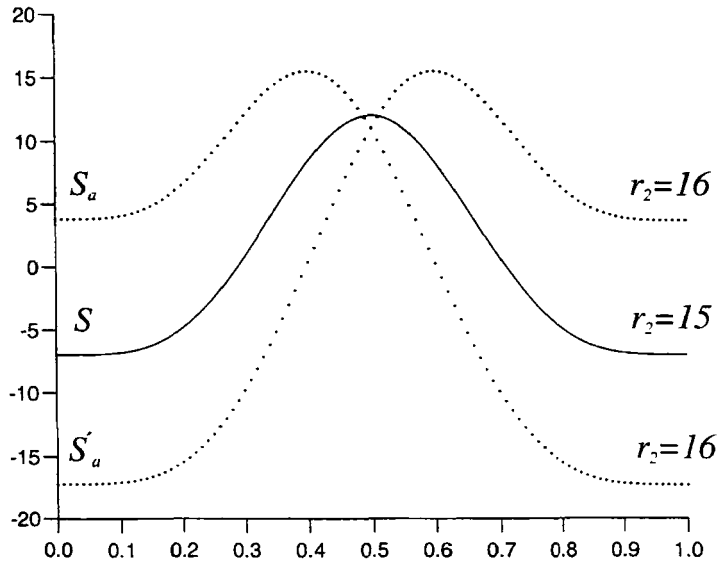

FIGURE 2 The mean velocity $\bar{u}$ is plotted against y, the width of the channel, showing the symmetric solution S at $r_2 = 15$ and two asymmetric solutions, S_a and S'_a, at $r_2 = 16$.

which is a plot of $\bar{u}$ against y. Also shown as dashed curves are the two asymmetric solutions found at $r_2 = 16$. Here, the bifurcation is of supercritical pitchfork type because the one symmetric stable solution for $r_2 < 15.22$ breaks at $r_2 = 15.22$ into two stable asymmetric solutions, indicated by S_a and S'_a on the bifurcation diagram Figure 3, which also illustrates the very complicated set of bifurcations that occur at larger r_2. This symmetry-breaking bifurcation is called the mean flow instability because it is the mean flow which loses its symmetry here (Or and Busse, 1987); the resulting flow is also called the "mixed-mode solution" (LBG89), since it combines modes of both symmetric and anti-symmetric type. LBG89 found two distinct mixed-mode solutions, which they called type I and type II solutions; the distinction was that the phase difference between the symmetric and antisymmetric parts of the solutions were different. In this study, as in BH93, we found only one mixed-mode solution, corresponding to LBG89's type I. There must be an unstable symmetric solution coming out of the bifurcation point at $r_2 = 15.22$ as shown, but this unstable solution cannot be computed from our time-dependent code; nevertheless, as can be seen in Figure 3 this branch subsequently restabilises at larger r_2 to give stable symmetric phenomena.

As r_2 is further increased, a third bifurcation occurs at the point $r_2 = 19.85$, and the two asymmetric steady branches, S_a and S'_a, become time-dependent *via* a supercritical Hopf bifurcation leading to the formation of stable limit cycles. Two asymmetric solutions S_a and S'_a related to each other by the symmetry (10) both become

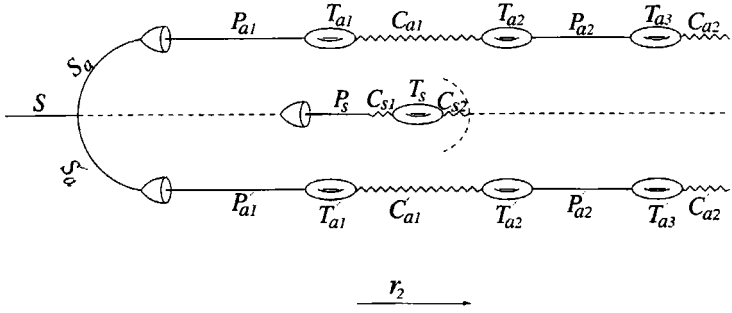

FIGURE 3 A schematic bifurcation diagram for the non-magnetic case with $P_r = 1$. The symbols S, P, T and C are for steady, periodic, torus, and chaos respectively. While the subscripts s and a are for symmetric and asymmetric respectively.

time-dependent at the same value of r_2. Figure 4 shows the S_a solution with $r_2 = 32$; $\bar{u}$ is plotted here against y at four equally spaced times during the cycle. We call these two asymmetric periodic solution branches P_{a1} and P'_{a1} on the bifurcation diagram, Figure 3. This transition to time-dependence in the mean flow was also found by both LBG89 and BH93. This time-dependent solution, called the vacillating solution by Schnaubelt and Busse (1992, 1997), was also found in small but finite E calculations with rigid boundaries; indeed they found that there is no great difference between no-slip and stress-free boundaries in this problem. The physical manifestation of this time-dependence is that the columnar rolls no longer drift steadily around the annulus, but undergo a periodic tilting as described in Figure 6 of BH93.

P_{a1} and P'_{a1} are the only solutions we found for $19.85 < r_2 < 33.15$, but just above $r_2 = 33.15$ a symmetric periodic stable state P_s was found (see Fig. 3). This spatio-temporal symmetry is described by $\bar{u}(y,t) = \bar{u}(1-y, t+T/2)$, $\widehat{\psi}(y,t) = \widehat{\psi}(1-y, t+T/2)$, $\bar{\theta}(y,t) = -\bar{\theta}(1-y, t+T/2)$ where T is the period of the oscillation. We

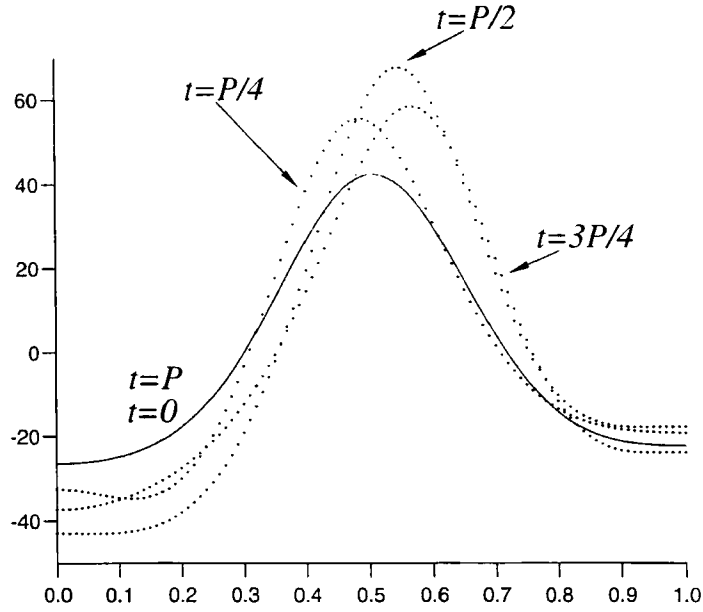

FIGURE 4 The asymmetric periodic behaviour of $\bar{u}$ at four equally spaced times of the period P.

conjecture that the unstable symmetric steady state emerging from the symmetry-breaking bifurcation undergoes a subcritical Hopf bifurcation leading to an unstable periodic symmetric solution at some $r_2 > 33.15$. This unstable branch restabilises in a saddle-node bifurcation at $r_2 = 33.15$ and this is where we first find this symmetric periodic solution, P_s. This scenario is consistent with the observation that as r_2 is reduced slowly down to 33.15 the symmetric solution suddenly disappears, rather than shrinking to zero. This suggests the subcritical behaviour conjectured above. Furthermore, the other two asymmetric solutions, P_{a1} and P'_{a1}, continue to exist for all parameter values $19.85 < r_2 < 35.27$, which means we have three stable solutions existing simultaneously as r_2 assumes the values from 33.15 to 35.27. This restabilisation of the symmetric states was not reported in either LBG89 or BH93, so this is the first qualitative difference in behaviour between the large but finite β studies and this study, where the asymptotic limit $\beta \to \infty$ has been taken.

3.2. More Complex Bifurcations

For higher values of r_2, the behaviour of the system is more complicated. At 35.27, the asymmetric periodic solutions of the mean velocity $\bar{u}$ undergo a bifurcation which introduces a second frequency to the limit cycles in P_{a1} and P'_{a1}. These therefore bifurcate into asymmetric 2-tori. Interestingly, 2-tori were found in the BH93 study, but were not reported by LBG89. A Poincaré return map of a section of one of the 2-tori is shown in Figure 5 for $r_2 = 35.285$. These 2-tori are designated in the bifurcation diagram Figure 3 as T_{a1} for the torus bifurcating from P_{a1}, and T'_{a1} for the one coming out of P'_{a1}. The 2-tori contain windows of frequency-locking as expected (*e.g.* Arn'old, 1983). Up to the appearance of the second frequency, our bifurcation scenario is similar to that found by Schnaubelt and Busse (1992, 1997). However, they found that chaos onset *via* periodic doubling bifurcation rather than the appearance and breakdown of a 2-torus as found here. They did, however, find the re-emergence of limit cycle behaviour at higher R_a as found here (Schnaubelt and Busse, 1997). They found a periodic symmetric oscillation (P_s in our notation) at Rayleigh number above that for the onset for chaos. The 2-torus structure prevails in the interval $35.3 < r_2 < 40$ before chaotic

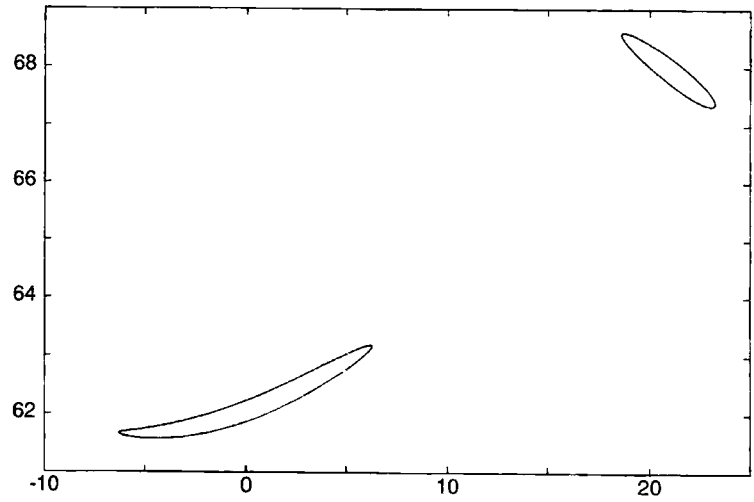

FIGURE 5 A Poincaré section of the torus T_{a1} at $r_2 = 35.285$.

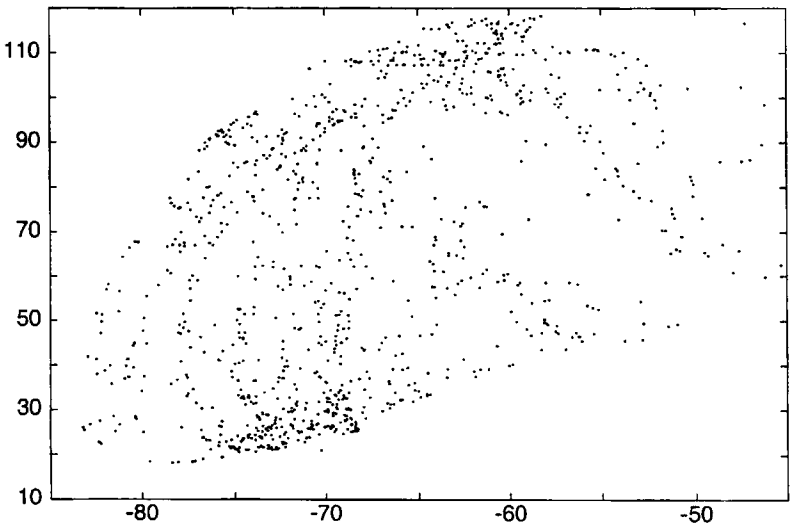

FIGURE 6 A Poincaré section showing the asymmetric behaviour of the mean velocity at $r_2 = 43$.

behaviour ensues for $r_2 > 40$. We call this chaotic motion C_{a1} on Figure 3. A Poincaré section of this chaotic motion is shown in Figure 6 at $r_2 = 43$. The same transition to chaos is taking place for the

second asymmetric solution, which we call C'_{a1}. Both types of chaos can be found, depending on the initial conditions.

A chaotic behaviour emerges from the symmetric solution P_s too, but for a lower value of the parameter r_2. This chaotic solution, C_{s1}, marks the behaviour of the solution for a small interval, namely $41.805 < r_2 < 41.993$; a Poincaré section of this symmetric chaos is given in Figure 7. It is of interest to compare the symmetric chaos shown in Figure 7 with the asymmetric chaos shown in Figure 6. Although the r_2 values are not too dissimilar, the solutions are clearly distinct. As r_2 is increased along the symmetric branch, the chaos bifurcates into a symmetric 2-torus T_s shown in Figure 8, at $r_2 = 42$. Then, at $r_2 = 42.09$ the 2-torus T_s again becomes chaotic. This chaotic behaviour characterizes the symmetric solution at C_{s2} up until $r_2 = 43$. Note, however, that despite all these bifurcations, the symmetric structure is maintained for all solutions coming out of the bifurcation point at $r_2 = 33.15$ on the symmetry line P_s on the bifurcation diagram Figure 3. However, symmetric solutions could not be found for $r_2 > 43$; the symmetric branch of solutions appears to terminate here.

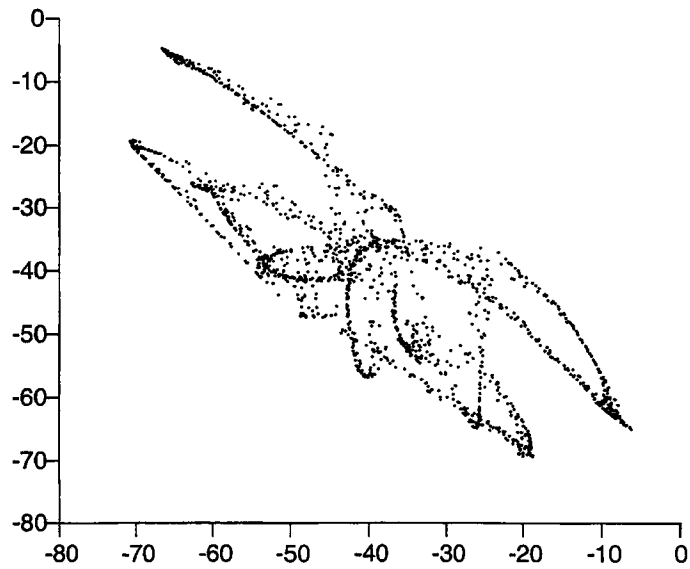

FIGURE 7 The symmetric chaotic solution found at $r_2 = 41.9$ is shown in this Poincaré return map of the projected trajectories of $\bar{u}$.

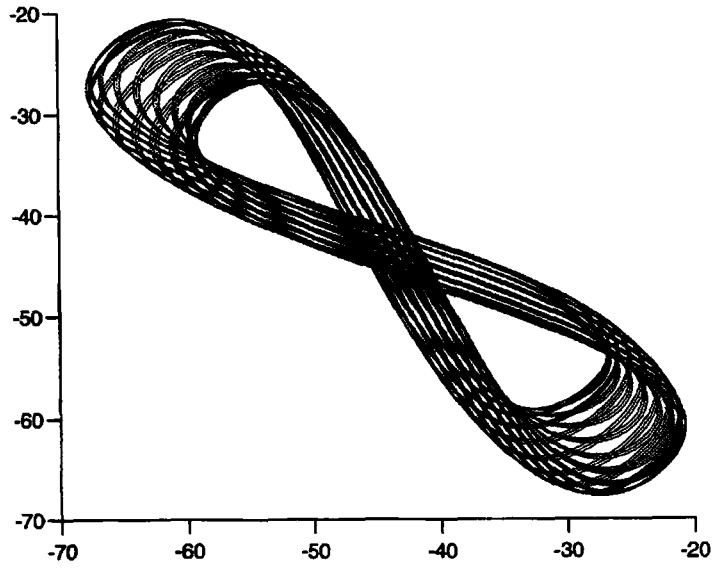

FIGURE 8 The symmetric 2-torus, T_s, for $\bar{u}$ at $r_2 = 42$.

Increasing r_2 slightly above 43 while on C_{s2} always resulted in an asymmetric solution.

The two asymmetric aperiodic solutions, C_{a1} and C'_{a1}, remain aperiodic for all the values $40 < r_2 < 45$. As r_2 is further increased, the chaotic solutions C_{a1} and C'_{a1} restabilise into asymmetric 2-tori, T_{a1} and T'_{a1}, at $r_2 = 45$; one of these is shown at $r_2 = 46$ in Figure 9. Periodic windows are expected in 2-tori, and indeed frequency-locking was found, for example, in the interval $45.144 < r_2 < 45.153$. An example of a frequency locked solution at $r_2 = 45.15$ is shown in Figure 10; its relationship to Figure 9, which is close in the parameter space, is clear. The asymmetric doubly periodic solutions, T_{a2} and T'_{a2}, continue to exist up to $r_2 = 46.7$, then at each asymmetry branch, periodic windows of stable asymmetric solutions, P_{a2} and P'_{a2}, for the values $46.7 < r_2 < 56$ appear where order to the system is restored and the 2-torus becomes a simple limit cycle again.

The singly periodic solutions, P_{a2} and P'_{a2}, become doubly periodic at $r_2 = 56$, giving rise to the 2-tori T_{a3} and T'_{a3} before bifurcating to chaotic solutions C_{a2} and C'_{a2} near $r_2 = 58$. The behaviour appears to remain chaotic at larger values of r_2; we have tested up to $r_2 = 100$.

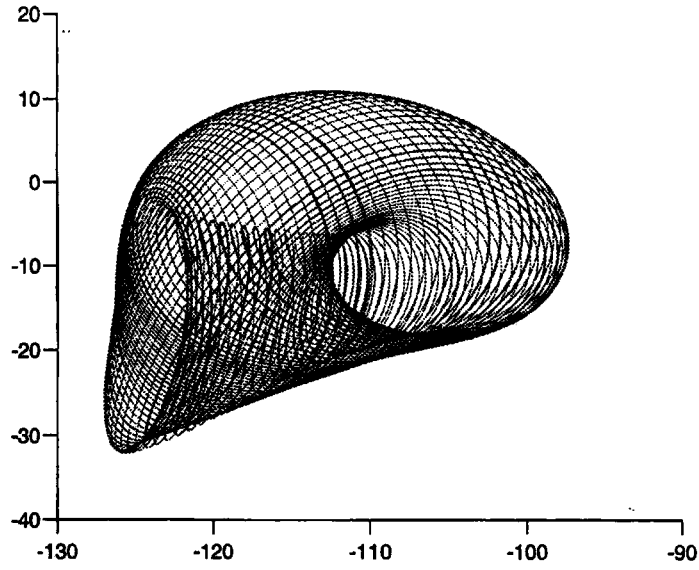

FIGURE 9 The asymmetric solution for $\bar{u}$ projected on the mean velocity plane showing one of the asymmetric 2-tori, T_{a2}, at $r_2 = 46$.

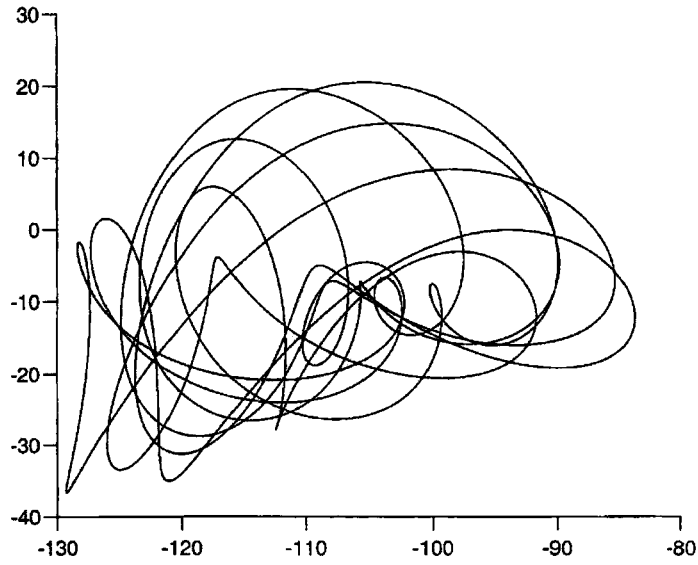

FIGURE 10 The frequency in the 2-torus T_{a2} is now locked at $r_2 = 45.15$.

3.3. Non-magnetic Convection at Varying Prandtl Number

We have investigated the behaviour of our non-magnetic system at Prandtl numbers other than 1, but for practical reasons it is not possible to do such a complete summary as was done for the Prandtl number 1 case.

The bifurcation sequence at higher Prandtl numbers is somewhat different from the $P_r = 1$ case described above. As r_2 is increased, we first find steady symmetric states, as at $P_r = 1$. However, the onset of the symmetry-breaking mean flow instability is deferred at larger Prandtl numbers, and the symmetric steady state bifurcates directly to a periodic state, which consists of an oscillation about a symmetric state. This is illustrated in Figure 11, which is for $r_2 = 55$. At $P_r = 5$, this Hopf bifurcation occurs just below $r_2 = 35$. This periodic state persists until just below $r_2 = 59$, but just above this a symmetry-breaking bifurcation occurs, and the oscillation is now around an asymmetric state, rather than a symmetric state. A similar bifurcation sequence was found at $P_r = 10$.

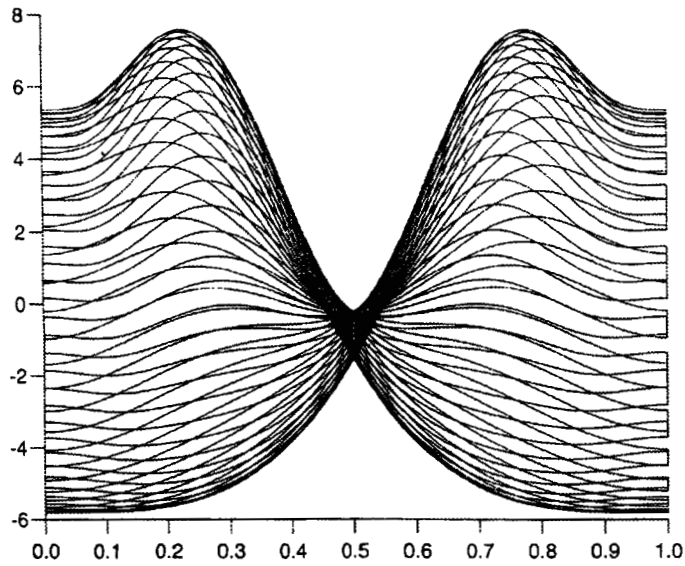

FIGURE 11 Plot of the oscillation of the non-magnetic solution at $r_2 = 55$ with $P_r = 5$.

As the Rayleigh number is further increased at $P_r = 5$, chaotic behaviour was found to onset just beyond $r_2 = 76$. Chaos appears to persist at higher r_2; we have tested up to $r_2 = 100$.

4. THE EFFECT OF MAGNETIC FIELD

4.1. Linear Theory of the Magnetoconvection Problem

In the magnetic case, we have two extra parameters, q and P_m in the problem. If the Prandtl numbers P_r and P_m are fixed, the Rayleigh number at the first bifurcation r_0 is now a function of the magnetic field strength q. The real and imaginary parts of the dispersion relation (4) now give

$$q(P_r - P_m) = (k^2 + c_0^2 P_m^2)\left[\frac{1}{k^2 c_0} - 1 - P_r\right], \tag{11}$$

$$r_0(P_r - P_m) = (k^2 + c_0^2 P_r^2)\left[\frac{1}{c_0} - k^2 - k^2 P_m\right], \tag{12}$$

from which r_0 and c_0 can be found as functions of q. As noticed by Soward (1979), the neutral curve of r_0 against q can have a complicated topology, with several different branches intersecting. The procedure for evaluating the neutral curve is, however, quite straightforward. Following Soward (1979), we introduce a variable γ which traces out the neutral curve from the following formulae

$$f(\gamma) = \frac{(\gamma - 4 - 4P_m)(\gamma - 1 - P_r)}{(\gamma + 2 + 2P_r)(\gamma - 1 - P_m)}, \tag{13}$$

$$\sigma = \frac{(f-1)(2P_m^2 - P_r^2) \pm \left[(1-f)^2(2P_m^2 + P_r^2)^2 + 36 f P_r^2 P_m^2\right]^{1/2}}{2(f+2)}, \tag{14}$$

$$c_0 = \sigma^{-1/3}\gamma^{-1/3}, \tag{15}$$

$$r_0 = \sigma^{2/3}\gamma^{-4/3}(1 + P_r^2/\sigma)(\gamma - 1 - P_m)/(P_r - P_m), \tag{16}$$

$$q = \sigma^{1/3}\gamma^{-4/3}(1 + P_m^2/\sigma)(\gamma - 1 - P_r)/(P_r - P_m), \tag{17}$$

The physical meanings of the variables σ and γ are $\sigma = k^2/c_0^2$, $\gamma = 1/k^2 c_0$ so only solutions with σ and r_0 positive are relevant. In some cases, it is possible for the negative sign in (14) to lead to an acceptable branch, but in most cases it is the positive sign which leads to minimum r_0.

Since it is not possible to cover the whole (P_r, P_m, q) space in detail, we have chosen some representative values to study. The case $P_r = P_m = 1$, which might be thought a natural starting place, is in fact singular as can be seen from (16). At $P_r = 1$, $P_m = 0.5$ the $(r_0 - q)$ neutral curve is simple, see the dotted curve in Figure 12, and a single point at $\gamma = 4$ corresponding to $q = 1.89$ and $r_0 = 1.49$ has been selected, so that case (i) has $P_r = 1$, $P_m = 0.5$ and $q = 1.89$.

At $P_r = 1$, $P_m = 5$ the situation is more complicated and (13)–(17) give two neutral curves, see the single-dash curves in Figure 12; we chose the point $\gamma = 1.8$ which corresponds to $q = 2.03$, $r_0 = 0.94$; and case (ii) is therefore $P_r = 1$, $P_m = 5$, $q = 2.03$.

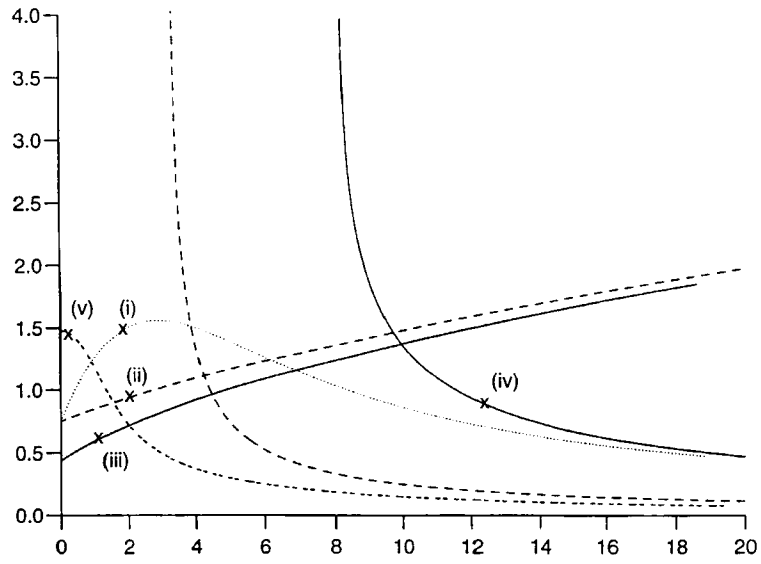

FIGURE 12 Neutral curves in the $(r_0 - q)$ plane. "....." $P_r = 1$, $P_m = 0.5$. Case (i) is at $q = 1.89$ and $r_0 = 1.49$: "- - - -" $P_r = 1$, $P_m = 5$. Case (ii) is at $q = 2.03$ and $r_0 = 0.94$: the two branches indicated by "————" both correspond to $P_r = 0.5$, $P_m = 1$. Case (iii) is at $q = 1.17$ and $r_0 = 0.61$ on the first branch and case (iv) with $q = 12.22$ and $r_0 = 0.91$ is on the second branch: "-- -- -- --" $P_r = 5$, $P_m = 0.5$. Case (v) is at $q = 0.26$ and $r_0 = 1.46$.

At $P_r = 0.5$, $P_m = 1$ there are again two neutral curves, which now intersect in the $(r_0 - q)$ plane, see solid curves in Figure 12. We wanted to look at a case on both branches, so $\gamma = 1.4$, $q = 1.17$, $r_0 = 0.61$ which gives the case (iii) and $\gamma = -18.5$, $q = 12.22$, $r_0 = 0.91$ gives the case (iv) both marked on Figure 12. Note that since $\gamma = 1/k^2 c_0$ this implies that the wave travels in the opposite direction in case (iv), *i.e.*, westwards rather than eastwards in a geophysical context.

At $P_r = 5$, $P_m = 0.5$, period doubling sequences leading to chaos were found. The dispersion curve in the $r_0 - q$ plane for $P_r = 5$, $P_m = 0.5$ is shown in Figure 12 by the double-dash curve, and the point chosen as case (v) is marked on the figure; $\gamma = 8$, $q = 0.26$ and $r_0 = 1.46$.

4.2. Nonlinear Behaviour for Cases (i) to (v)

In case (i) $P_r = 1$, $P_m = 0.5$, $q = 1.89$ this nonlinear behaviour is remarkably simple. As r_2 increases, the first bifurcation to a symmetric steady state occurs shortly after $r_2 = 10$, and there are no further bifurcations. The steady symmetric state persists up to at least $r_2 = 1000$; an example of the form of $\bar{u}$ can be seen at $r_2 = 200$ in Figure 13. In this case, therefore both the mean flow instability and the time-dependence have been completely suppressed by the magnetic field. This is a surprising result in view of the persistence of the appearance of the mean-flow instability in the non-magnetic case. All non-magnetic investigations of the problem in the literature, with a variety of different approaches, have found a mean flow instability. Note that in Figure 13 the mean flow is negative (westward) in the interior, positive near the boundaries, whereas in the non-magnetic case the mean flow is positive (eastward) in the interior (see, *e.g.*, Fig. 2). The stress free boundary conditions ensure that the integral of the mean flow over the annulus is zero. The change of sign seems to be related to the factor $1 - qP_m/(k^2 + c_0^2 P_m^2)$, which always becomes negative at sufficiently large q [the limit $\gamma \to \infty$ in Eqs. (13)–(17)].

In case (ii) $P_r = 1$, $P_m = 5$, $q = 2.03$, so magnetic diffusion is now the smallest of the three diffusivities. Now the first bifurcation to a symmetric steady state occurred at r_2 just below 5. As r_2 is increased, the next bifurcation is to a symmetric oscillation at $r_2 = 13$. At $r_2 = 13.93$ a further bifurcation occurs to an asymmetric oscillation. This behaviour resembles the non-magnetic $P_r = 5$ case considered in

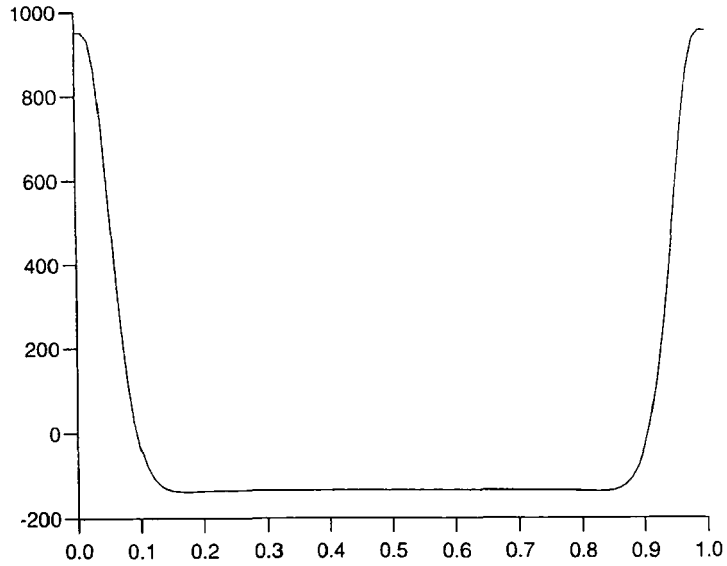

FIGURE 13 Plot of the symmetric steady state solution for the mean velocity $\bar{u}$ in the magnetic case at $r_2 = 200$ with $P_r = 1$, $P_m = 0.5$, $q = 1.89$ and $r_0 = 1.49$.

Section 3.3, rather than the $P_r = 1$ bifurcation sequence. However, at $r_2 = 17.5$ the asymmetric oscillation bifurcates back to a steady asymmetric state, but on further increasing $r_2 \approx 18$, periodicity returns. At larger r_2 a torus develops ($r_2 \approx 20.5$) followed by symmetric chaos ($r_2 \approx 25$). Asymmetric chaos is found at higher values of r_2.

In case (iii) $P_r = 0.5$, $P_m = 1$, $q = 1.17$, the first bifurcation to a symmetric state occurs at r_2 just below 4. The next bifurcation is now to an asymmetric steady state (mean-flow instability), and this is followed by asymmetric chaos *via* a torus. The bifurcation sequence in this case is generally similar to that for non-magnetic convection at $P_r = 1$.

In case (iv) $P_r = 0.5$, $P_m = 1$, $q = 12.22$ the first bifurcation to a symmetric steady state occurs at r_2 just below 105. As in case (a), this was the only bifurcation found. The flow remains steady and symmetric right up to 1000, the highest value of r_2 tested.

In case (v) $P_r = 5$ and $P_m = 0.5$ $q = 0.26$ the behaviour is rather different. After an initial bifurcation to a steady symmmetric state at $r_2 = 15$, the next bifurcation is to a steady asymmetric state at

$r_2 = 44.8$. This asymmetric state becomes oscillatory at $r_2 = 52$. Up to this point, the scenario is very similar to the non-magnetic $P_r = 1$ case. However, whereas that case developed into a 2-torus, this magnetic case (v) now goes through a period doubling sequence to chaos. This is illustrated in Figure 14 which shows succesive period doublings. The final chaotic state is achieved at $r_2 = 57$.

It is clear from the above results that many different bifurcation scenarios can occur at different parameter values. Certain trends are, however, evident from these runs, and others that we have considered. At sufficiently large magnetic field strength, q, the only bifurcation is the first one, to steady symmetric flow. A strong magnetic field suppresses all the symmetry breaking bifurcations and the time-dependence in this model. At large r_2 a boundary layer structure develops, with $\bar{u}$ becoming uniform in the interior (see Fig. 13). Generally, this suppression of secondary bifurcations is associated with the reversed mean flow (negative, *i.e.*, westward) in the interior. However, we did find examples where the field is strong enough to

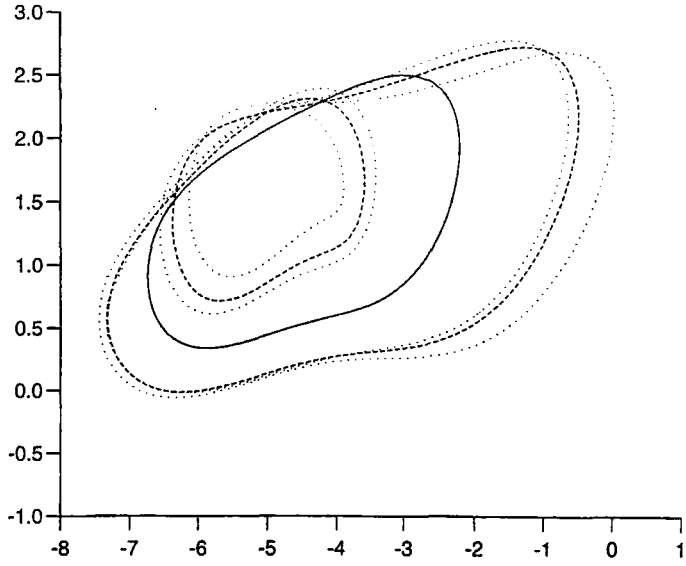

FIGURE 14 Phase plane of the mean velocity showing period doubling cascades; $P_r = 5$, $P_m = 0.5$ and $q = 0.26$. The solid curve at $r_2 = 55$; the dashed curve at $r_2 = 56$; the dotted curve at $r_2 = 56.2$.

suppress the secondary bifurcations but not strong enough to reverse the mean flow.

When secondary bifurcations occur, there are two main scenarios, depending on whether the symmetry breaking mean flow instability occurs first or whether the mean flow becomes time-dependent first. In either case, at sufficiently large r_2 the mean flow usually bifurcates to an asymmetric and time-dependent state. Again, at sufficiently large r_2 this time-dependent state is generally chaotic. In most parts of the parameter space we found transition to chaos takes place *via* the breakdown of a 2-torus state, as found by BH93, but in case (v) we found chaos from a period doubling scenario, as in the truncated LBG89 equations; we have not found period doubling in the non-magnetic system.

5. CONCLUSIONS

The large wavenumber approximation provides a very significant simplification to the annulus model, while still retaining the possibility of investigating behaviour at large Rayleigh number. Comparison of the non-magnetic results with those of fully two-dimensional computations suggest that the features which were robust in those calculations, such as the mean flow instability and the appearance of periodic oscillations of the mean flow, also occur in this asymptotic approach. Some of the behaviour found in the two-dimensional simulations of BH93, such as the appearance of 2-tori and chaotic solutions also occur here, but these higher transitions are less robust, in the sense that they are more dependent on the exact location in parameter space. One aspect which is lost in this large wavenumber analysis is the possibility of transitions between wavenumbers, which was noted by BH93.

Because we have been able to explore a wider range of parameter space than is possible with two-dimensional simulations a number of new bifurcation sequences have been found. A possibility that occurs both in non-magnetic and magnetic convection is the onset of periodic oscillation in the mean-flow before the appearance of the symmetry-breaking "mean-flow" instability. We find that in most cases where there is no magnetic or only a weak magnetic field, that at large r_2 the flow is in a chaotic state, the most common route to chaos (though not

the universal route) being through the breakdown of a 2-torus. We have also found that both symmetric and asymmetric solutions can be found in the same region of parameter space, and that in some areas of parameter space distinct chaotic attractors exist, one of which is symmetric and two others are asymmetric.

We find that a magnetic field can suppress the secondary bifurcations provided that it is sufficiently strong; q has to be large compared to O(1). Since $\beta \sim E^{-1}$, where E is the Ekman number, and our scaling is only valid at large β (small E) this means that the Chandrasekhar number Q must be large compared to $O(E^{-2/3})$ which in turn implies that the Elsasser number is large compared to $O(E^{1/3})$. This is in the geophysically interesting range; recent dynamo simulations suggest that the Elsasser number can become of order unity, while the convection cells still can have the columnar structure which our analysis presupposes.

The annulus model is often viewed as a simplification of full spherical geometry, and it has been shown recently that the annulus approximation gives good results compared with the linear non-magnetic problem of convection in a sphere despite the assumption that the slope on the endwalls is small (Jones *et al.*, 2000; Yano, 1992). Whether this result persists to higher Rayleigh numbers is not yet known, but at least the annulus model, which is much more tractable than the full spherical problem, gives a basis for comparison. In the magnetic case, the strength of the field is significant. If the field is weak, *i.e.*, the Elsasser number is less than $O(E^{1/3})$, the field has very little effect. The annulus model is most useful for fields with Elsasser number of the order $O(E^{1/3})$, and will break down when the field becomes strong, *i.e.*, Elsasser number O(1). When the Elsasser number is O(1), the flow becomes fully three-dimensional and the annulus geometry loses much of its attraction. However, numerical studies (*e.g.* Zhang and Jones, 1994) suggest that typically the Elsasser number has to be O(10) before the effects of the Taylor-Proudman constraint are fully overcome, so that the annulus model may be useful for a significant range of magnetic field strengths.

References

Arn'old, V. I., *Geometrical Methods in the Theory of Ordinary Differential Equations*, Springer-Verlag, New York/Berlin/Heidelberg/Tokyo (1983).

Bassom, A. P. and Zhang, K., "Strongly nonlinear convection cells in a rapidly rotating fluid layer," *Geophys. Astrophys. Fluid Dynam.* **76**, 223–238 (1994).

Brummel, N. H. and Hart, J. E., "High Rayleigh number β-convection," *Geophys. Astrophys. Fluid Dynam.* **68**, 85–114 (1993).
Busse, F. H., "Thermal instabilities in rapidly rotating systems," *J. Fluid Mech.* **44**, 441–460 (1970).
Busse, F. H., "Generation of planetary magnetism by convection," *Phys. Earth Planet Int.* **12**, 350–358 (1976).
Busse, F. H., "A model of mean zonal flow in the major planets," *Geophys. Astrophys. Fluid Dynam.* **23**, 153–174 (1983).
Busse, F. H., "Asymptotic theory of convection in a rotating, cylindrical annulus," *J. Fluid Mech.* **173**, 545–556 (1986).
Busse, F. H., "Convection driven zonal flows and vortices in the major planets," *CHAOS* **4**, 123–134 (1994).
Busse, F. H. and Or, A. C., "Convection in a rotating cylindrical annulus: thermal Rossby waves," *J. Fluid Mech.* **166**, 173–187 (1986).
Carrigan, C. R. and Busse, F. H., "An experimental and theoretical investigation of the onset of convection in rotating spherical shells," *J. Fluid Mech.* **126**, 287–305 (1983).
Guckenheimer, J. and Holmes, P., *Nonlinear oscillations, Dynamical Systems, and Bifurcations of Vector Fields*, Springer-Verlag, New York/Berlin/Heidelberg/Tokyo, 453 pp. (1983).
Hart, J. E., Glatzmaier, G. A. and Toomre, J., "Space-laboratory and numerical simulations of thermal convection in a rotating hemispherical shell with radial gravity," *J. Fluid Mech.* **173**, 519–544 (1986).
Jones, C. A., "Convection driven geodynamo models," *Phil. Trans. R. Soc. Lond.* A **358**, 1–25 (2000).
Jones, C. A., Soward, A. M. and Mussa, A. I., "The onset of convection in a rapidly rotating sphere," *J. Fluid Mech.* **405**, 157–179 (2000).
Lin, R.-Q., Busse, F. H. and Ghil, M., "Transition to two-dimensional turbulent convection in a rapidly-rotating annulus," *Geophys. Astrophys. Fluid Dynam.* **45**, 131–157 (1989).
Olson, P. and Glatzmaier, G., "Magnetoconvection in a rotating spherical shell; structure of flow in the outer core," *Phys. Earth Planet Int.* **95**, 109–118 (1995).
Or, A. C. and Busse, F. H., "Convection in a rotating cylindrical annulus. Part 2. Transitions to asymmetric and vacillating flow," *J. Fluid Mech.* **174**, 313–326 (1987).
Petry, M., Busse, F. H. and Finocchi, F., "Convection in a rotating cylindrical annulus in the presence of a magnetic field," *Eur. J. Mech B/Fluids* **16**, 817–833 (1997).
Roberts, P. H., "On the thermal instability of a rotating fluid sphere containing heat sources," *Phil. Trans. R. Soc. Lond.* A **263**, 93–117 (1968).
Schnaubelt, M. and Busse, F. H., "Convection in a rotating cylindrical annulus. Part 3. Vacillating and spatially modulated flows," *J. Fluid Mech.* **245**, 155–173 (1992).
Schnaubelt, M. and Busse, F. H., "Thermal convection in the rotating cylindrical annulus," *Acta Astron. et Geophys. Univ. Comenianae*, **19**, 63–78 (1997).
Soward, A. M., "On the finite amplitude thermal instabilities of a rapidly rotating fluid sphere," *Geophys. Astrophys. Fluid Dynam.* **9**, 19–74 (1977).
Soward, A. M., "Convection driven dynamos," *Phys. Earth Planet Int.* **20**, 134–151 (1979).
Sun, Z. P., Schubert, G. and Glatzmaier, G. A., "Transitions to chaotic thermal convection in a rapidly rotating spherical fluid shell," *Geophys. Astrophys. Fluid Dynam.* **69**, 95–131 (1993).
Yano, J.-I., "Asymptotic theory of thermal convection in rapidly rotating systems," *J. Fluid Mech.* **243**, 103–131 (1992).
Zhang, K., "Convection in a rapidly rotating spherical shell at infinite Prandtl number: steadily drifting rolls," *Phys. Earth and Planet Int.* **68**, 156–169 (1991).
Zhang, K. and Jones, C. A., "Convective motions in the Earth's fluid core," *Geophysical Research Letters* **21**, 1939–1942 (1994).